International Journal of Fatigue 83 (2016) 36–41

Contents lists available at ScienceDirect

International Journal of Fatigue

journal homepage: www.elsevier.com/locate/ijfatigue

Gaussian specimens for VHCF tests: Analytical prediction of damping effects

A. Tridello *, D.S. Paolino, G. Chiandussi, M. Rossetto

Department of Mechanical and Aerospace Engineering, Politecnico di Torino, 10129 Turin, Italy

ARTICLE INFO

Article history:
Received 30 October 2014
Received in revised form 22 April 2015
Accepted 29 April 2015
Available online 15 May 2015

Keywords:
Gigacycle fatigue
Very-high-cycle fatigue
Risk-volume
Ultrasonic testing machine
Power dissipated

ABSTRACT

Experimental tests investigating Very-High-Cycle Fatigue (VHCF) properties of materials are commonly performed with ultrasonic testing machines which allow for a significant reduction of testing time but induce a relevant temperature increment in specimens. In particular, due to the large volume of material (risk-volume) under test, Gaussian specimens, recently introduced for investigating size effects in VHCF, are extremely prone to heat dissipation and to the consequent temperature increment. They were originally designed by the Authors without considering the hysteretic damping and its effects on power dissipation: however, in order to evaluate the feasibility of ultrasonic fatigue tests with Gaussian specimens, hysteretic damping effects must be taken into account.

The paper proposes an analytical model that permits to evaluate the effects of the hysteretic damping on the distribution of the power density and on the power dissipation in Gaussian specimens. The theoretical model is verified through Finite Element Models and experimentally validated.

1. Introduction

In recent years, Very-High-Cycle Fatigue (VHCF) behavior of metallic materials has become a major point of interest for researchers and industries. The needs of specific industrial fields (aerospace, mechanical and energy industry) for structural components with increasingly large fatigue lives, up to 10^{10} cycles (gigacycle fatigue), requested for a more detailed investigation on the experimental properties of materials in the VHCF regime.

Gigacycle fatigue tests are commonly performed using resonance testing machines [1,2] with a loading frequency of 20 kHz (ultrasonic tests). Experimental results on high-strength steels showed that, depending on the stress amplitude, failures may be due to two different types of crack nucleation [3]. If the stress amplitude is above the conventional fatigue limit, cracks nucleate at the specimen surface (surface nucleation); if the stress amplitude is below the conventional fatigue limit, cracks nucleate from inclusions or internal defects (internal nucleation). Following the experimental evidence, new phenomenological models were introduced [4] for the description of the fatigue life. With the proposed models, the random occurrence of superficial and internal failures and the possible presence of a VHCF fatigue limit can be described in a statistical framework.

Together with the introduction of new fatigue life models, research on VHCF focused on the effect of different factors influencing material response (e.g., stress ratio [5,6], load type [7], environment conditions [8]). Recently, size-effect gained significant attention. In particular, specimens with different risk-volumes (specimen volume subjected to a stress amplitude larger than the 90% of its maximum value) were investigated [9–11]. Experimental results showed that, in case of high-strength steels, the larger the risk-volume the smaller the fatigue strength. As a consequence, for a conservative evaluation of VHCF properties, VHCF tests should be run with specimens characterized by large risk-volumes. However, a significant increment of the risk-volume is not possible with common specimen shapes used for VHFC tests (hourglass or dog-bone). With hourglass specimens, limited risk-volumes (less than 200 mm^3) can be tested and with dog-bone specimens, moderate risk-volumes (less than 2000 mm^3) can be tested, due the non-uniform stress distribution along the specimen part with constant cross section.

A further increment of the risk-volume was obtained by the Authors [12] with the adoption of Gaussian specimens (Fig. 1). In Gaussian specimens, the profile of the central specimen part entails the Gaussian form, which provides an almost uniform stress distribution and consequently allows for testing large risk-volumes (up to 20,000 mm^3). Gaussian specimens can be designed

* Corresponding author at: C.so Duca degli Abruzzi 24, Department of Mechanical and Aerospace Engineering, Politecnico di Torino, 10129 Turin, Italy. Tel.: +39 011 090 6913; fax: +39 011 090 6999.

E-mail addresses: andrea.tridello@polito.it (A. Tridello), davide.paolino@polito.it (D.S. Paolino), giorgio.chiandussi@polito.it (G. Chiandussi), massimo.rossetto@polito.it (M. Rossetto).

http://dx.doi.org/10.1016/j.ijfatigue.2015.04.025
0142-1123/

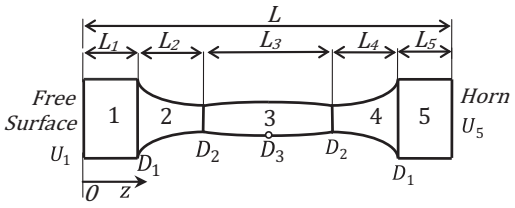

Fig. 1. Typical Gaussian specimen.

according to the analytical procedure described in [12]. Numerical and experimental tests were carried out in [12,13] in order to compare the risk-volumes attainable with Gaussian and dog-bone specimens. The results confirmed that dog-bone specimens are appropriate for moderate risk volumes, while the Gaussian shape allows to design specimens with large risk-volumes.

The design of Gaussian specimens in [12] was carried out without taking into account the hysteretic damping and its effect on power dissipation. However, as the risk-volume increases, hysteretic damping effects cannot be neglected and must be taken into account in order to assess the feasibility of ultrasonic tests with Gaussian specimens.

The present paper proposes an analytical model for the prediction of the stress distribution and of the power dissipation in Gaussian specimens with hysteretic damping. The analytical model is numerically verified through a Finite Element Analysis (FEA) by considering Gaussian specimens with risk-volumes ranging from 1000 mm^3 to 5200 mm^3 and is experimentally validated by using a Gaussian specimen with a 2000 mm^3 risk-volume.

2. Gaussian specimen with hysteretic damping: Analytical models

Internal dissipation in Gaussian specimens is modeled by considering a hysteretic damping model. The complex elastic modulus, E_d ($E_d = E_r(1 + \mathbb{i}\eta)$), is introduced in order to take into account the hysteretic damping: the real part of the elastic modulus, E_r, takes into account the elastic energy stored by the vibrating body, while the imaginary part ηE_r, being η the loss factor, takes into account the amount of energy dissipated due to internal dissipation. In presence of hysteretic damping, a closed-form solution for the stress distribution in the Gaussian specimen part cannot be determined. Therefore, the Gaussian profile is approximated with a cosine function (Section 2.1), which allows for the computation of the stress distribution along the longitudinal axis of the specimen (Section 2.2). Finally, the power density dissipated along the longitudinal axis and the power dissipation are analytically determined (Section 2.3).

2.1. Approximation of the Gaussian profile

The Gaussian profile is obtained from the Webster's equation and by considering a uniform stress distribution in specimen part 3 (Fig. 1) without considering hysteretic damping [12]. If the hysteretic damping is introduced in the model, the elastic modulus and, consequently, the wave number become complex quantities. In case of complex wave number, the displacement amplitude in the Gaussian specimen part cannot be determined in a closed form. A closed form solution for the displacement amplitude can be obtained by approximating the Gaussian profile with a cosine function. The approximating cosine function that describes the cross-section diameter, $D(z)$, can be obtained by imposing the passage through points $(L_1 + L_2; D_2)$ and $(L/2 = L_1 + L_2 + L_3/2; D_3)$ as defined in Fig. 1. The approximating cosine function is given by:

$$D(z) = D_3 \cos\left[\alpha_3\left(z - \frac{L}{2}\right)\right], \tag{1}$$

where $\alpha_3 = 2\,\mathrm{acos}\left[\frac{D_2}{D_3}\right]\Big/L_3$ is a geometrical parameter introduced in order to guarantee the passage of the cosine approximating function through points $(L_1 + L_2; D_2)$ and $(L/2; D_3)$. The difference between the exact profile and the approximated profile is limited.

2.2. Analytical stress distribution

In presence of hysteretic damping, the stress and the strain amplitude are slightly out of phase. In the literature [14], the phase delay is analytically modeled with a complex elastic modulus, which yields to a complex wave number. A complex wave number, in the Webster's equation, finally yields to a complex displacement amplitude. Therefore, the imaginary part of the displacement amplitude allows for theoretically modeling the dissipated energy in a hysteretic cycle.

Eq. (2) reports the complex displacement amplitude in each specimen part ($j = 1, \ldots, 5$ in Fig. 1). Complex displacement amplitude for a straight profile (specimen part 1 and 2) and complex displacement amplitude for a circular profile approximated through an hyperbolic profile (specimen part 2 and 4) are determined according to [1]. The constant coefficients involved in the equations are necessarily complex quantities. The displacement amplitude in specimen part 3 is obtained by solving the Webster's equation for the cosine profile (Eq. (1)).

$$\begin{cases} u_1[z_1] = (A_{1r} + \mathbb{i}A_{1\mathbb{i}})\cos[kz_1] + (B_{1r} + \mathbb{i}B_{1\mathbb{i}})\sin[kz_1], & 0 \leqslant z_1 \leqslant L_1 \\ u_2[z_2] = \frac{(A_{2r}+\mathbb{i}A_{2\mathbb{i}})\cos\left[z_2\sqrt{k^2-\alpha_2^2}\right]+(B_{2r}+\mathbb{i}B_{2\mathbb{i}})\sin\left[z_2\sqrt{k^2-\alpha_2^2}\right]}{\cosh[\alpha_2(z_2-L_2)]}, & 0 \leqslant z_2 \leqslant L_2 \\ u_3[z_3] = \frac{(A_{3r}+\mathbb{i}A_{3\mathbb{i}})\cos\left[z_3\sqrt{k^2+\alpha_3^2}\right]+(B_{3r}+\mathbb{i}B_{3\mathbb{i}})\sin\left[z_3\sqrt{k^2+\alpha_3^2}\right]}{\cos[\alpha_3(z_3-\frac{L_3}{2})]}, & 0 \leqslant z_3 \leqslant L_3, \\ u_4[z_4] = \frac{(A_{4r}+\mathbb{i}A_{4\mathbb{i}})\cos\left[z_4\sqrt{k^2-\alpha_2^2}\right]+(B_{4r}+\mathbb{i}B_{4\mathbb{i}})\sin\left[z_4\sqrt{k^2-\alpha_2^2}\right]}{\cosh[\alpha_2 z_4]}, & 0 \leqslant z_4 \leqslant L_4 \\ u_5[z_5] = (A_{5r} + \mathbb{i}A_{5\mathbb{i}})\cos[kz_5] + (B_{5r} + \mathbb{i}B_{5\mathbb{i}})\sin[kz_5], & 0 \leqslant z_5 \leqslant L_5 \end{cases} \tag{2}$$

where $u_j[\cdot]$ denotes the displacement amplitude in each specimen part ($j = 1 \ldots 5$), $k = 2 \cdot \pi \cdot f_0 \Big/ \sqrt{\frac{E_d}{\rho}}$, being f_0 the resonance frequency and ρ the density, $\alpha_2 = \mathrm{acosh}[N_2]/L_2$, being N_2 the ratio D_1/D_2 and A_{jr}, B_{jr}, $A_{j\mathbb{i}}$ and $B_{j\mathbb{i}}$ ($j = 1, \ldots, 5$) are the 20 complex coefficients that can be determined by imposing proper boundary conditions (Appendix A).

At the free specimen surface ($z = 0$), the real part of the displacement amplitude is equal to U_1 (Fig. 1), while the imaginary part of the displacement amplitude and the real and imaginary parts of the strain amplitude are equal to 0:

$$\begin{cases} u_{1r}[z_1 = 0] = U_1 \\ u_{1\mathbb{i}}[z_1 = 0] = 0 \\ \varepsilon_{1r}[z_1 = 0] = 0 \\ \varepsilon_{1\mathbb{i}}[z_1 = 0] = 0 \end{cases}, \tag{3}$$

where $u_{jr}[\cdot]$ and $u_{j\mathbb{i}}[\cdot]$ denote the real and imaginary parts of the displacement amplitude in the jth specimen part and $\varepsilon_{jr}[\cdot]$ and $\varepsilon_{j\mathbb{i}}[\cdot]$ denote the real and imaginary parts of the strain amplitude in the jth specimen part. The other constant coefficients are determined